Article

Effect of Air Annealing on the Structural, Textural, Magnetic, Thermal and Luminescence Properties of Cerium Fluoride Nanoparticles

Vladislav Ilves [1,*], Aidar Murzakaev [1,2], Sergey Sokovnin [1,2], Tat'yana Sultanova [2], Olga Svetlova [2], Mikhail A. Uimin [2,3], Maria Ulitko [2] and Mikhail Zuev [4]

[1] Institute of Electrophysics, UB RAS, Yekaterinburg 620016, Russia
[2] Institute of Physics and Technology, Ural Federal University, Yekaterinburg 620002, Russia
[3] M.N. Mikheev Institute of Metal Physics, UB RAS, Yekaterinburg 620137, Russia
[4] Institute of Solid State Chemistry Ural Branch RAS, Yekaterinburg 620041, Russia
* Correspondence: ilves@iep.uran.ru

Abstract: This paper presents the physicochemical characteristics of CeF_3 nanopowder (NP) obtained via electron evaporation. The initial NP was annealed in air (200–500 °C) for 30 min. The annealed NP was evaluated using the following methods: X-ray diffraction (XRD), high-resolution transmission electron microscopy (HRTEM), differential scanning calorimetry-thermogravimetry (DSC-TG) and luminescence/magnetic measurements. The degree of cytotoxicity of CeF_3 nanoparticles (NPles) to cell cultures was determined. The cubic phase CeO_2 formed in CeF3 NP after annealing (500 °C). The appearance of the CeO_2 oxide phase led to an increase in the intensity of photoluminescence. Cathodoluminescence was not excited. The paramagnetic response of NPles decreased with an increase in the annealing temperature. Cerium fluoride NPles showed low cytotoxicity towards cancerous and non-cancerous cells. Annealing of the CeF_3 NP at low temperatures led to an improvement in the textural parameters of the not annealed NP. Improved texture parameters indicate the prospect of using CeF_3 as a biomedicine nanocontainer.

Keywords: CeF_3 nanoparticles; annealing; pulsed electron beam evaporation

1. Introduction

Numerous experimental [1,2] and theoretical works [3,4] confirm the presence of ferromagnetism at room temperature in cerium oxide nanoparticles (NPles). Prospects for the use of CeO_2 NPles in biomedicine are shown in a number of comprehensive reviews [5,6] and monographs [7,8]. No less interesting are the prospects for the use of NPle fluorides, in particular CeF_3 in medicine [9]. Recently, [10] showed that CeO_2/CeF_3 composite NPles (composites were synthesized by fluorination of initial CeO_2 nanoparticles) showed an increase in the saturation magnetization in the CeO_2/CeF_3 NPles compared to the initial, vacuum and air-annealed CeO_2 NPles. According to the authors of the article [10], the most plausible explanation of the origin of ferromagnetism in composite CeO_2/CeF_3 powder consists of the presence of defects in the interface between composite CeO_2 and CeF_3 structures. Based on the above idea of the origin of room-temperature ferromagnetism (RTFM) on the "fluoride oxide" interface of the composite, we decided to test the possibility of an ferromagnetic (FM) response as a result of the formation of an oxide shell from CeO_2 during annealing in air on the surface of paramagnetic CeF_3 NPles after their annealing in air (previously, we experimentally observed FM response in pure CeO_2 and Cu (C, Fe)-doped CeO_2 NPles [11] and paramagnetism NPles CeF_3 [12]). Early studies of phase transformation of CeF_3 during annealing in air [13] showed that a noticeable amount of CeO_2 is formed in the CeF_3 powder only after annealing at a temperature of 600–700 °C, which was confirmed by X-ray diffraction (XRD) analysis. We decided to anneal the CeF_3

NPles in air produced earlier by the pulsed electron beam evaporation (PEBE) method in a vacuum [12], in order to induce in CeF_3-CeO_2 NPles RTFM on the "fluoride-oxide" interface without using gas fluorination and in parallel with studying the physicochemical characteristics of the annealing core–shell NPles CeF_3 (core)-CeO_2 (shell). Studies of nucleus–shell structures show their intense luminescence and biocompatibility [14,15]. The core–shell structures are attractive due to their remarkable physicochemical characteristics, such as thermal stability, improved solubility in water, etc. [16–18]. For example, water-soluble Luminescent Silica-Coated Cerium Fluoride Nanoparticles were successfully synthesized in [14]. The cytotoxic test showed that CeF_3: Tb @ LaF_3 @ SiO_2 NPs have minimum toxicity with respect to CeF_3: Tb @ LaF_3 NPs and the control drug dasatinib on HT-29 and HepG2 cell lines. The authors [16] recommended NPles CeF_3: Tb @ LaF_3 @ SiO_2 for use in biomedical research, including biomarking, biodetection, biosonding, cell and tissue labeling, bioimaging, drug delivery, cancer treatment and multiplex analysis. In turn, the luminescent and magnetic properties of lanthanide NPles play a fundamentally important role in the design of multifunctional nanomaterials, allowing them to be used in magnetic resonance therapy and other luminescent methods, including for deep tissue imaging and low-resolution imaging [16,17]. The results of the present work showed that air annealing of CeF_3 NPles did not lead to an FM response on the «fluoride–oxide» interface. It is possible that the concentration of defects on the interface was insignificant for inducing FM response; therefore, in the future, we assume defects will be created along the boundaries of the CeF_3-CeO_2 NPle grains via irradiation with high-energy electrons (700 keV) on a pulsed-periodic accelerator URT-0.5 [19]

2. Results and Discussion

Mesoporous amorphous crystal CeF_3 NP was prepared using the PEBE method; evaporation mode and basic physical and chemical characteristics of CeF_3 NPles are described in [12]. Annealing of CeF_3 micron and nano powders was carried out in air at 200, 300 and 500 °C in an electric furnace chamber PKL 1.2–12 in alundum crucible for 30 min. The evolution of the color of CeF_3 NP from the annealing temperature is shown in Figure 1a. NP, after annealing at 500 °C, acquired a brighter color than the color of unannealed micron powder (sample SM0). The change in NP color indirectly proves that the dark color (the color of NP: coffee with milk) of the original CeF_3 NP (sample S0) was not caused by an impurity of an unspecified oxofluoride phase, but was associated with a large number of all kinds of structural defects and a small amount of metal Ce NPles, recovered by evaporation at high temperature under vacuum conditions. A similar evolution in the NP color was observed by us earlier during annealing in the air of CaF_2 NP, also obtained by PEBE in a vacuum [20]. A change in the color of commercial micron powder with an increase in the annealing temperature (Figure 1b) was not visually observed.

Figure 1. (**a**) Change in the color of the CeF3 NP (sample S0) from the annealing temperature in air; (**b**) color change in SM0 sample from commercial powder (Cerium (III) fluoride-anhydrous powder, 99.99% trace metal basis, Sigma-Aldrich) from air-annealing temperature.

X-ray diffractograms of the original unannealed CeF_3 micro and nano powders (samples SM0 and S0) were annealed at 200, 300 and 500 °C NP S0 (samples S200, S300 and S500) and are shown in Figure 2.
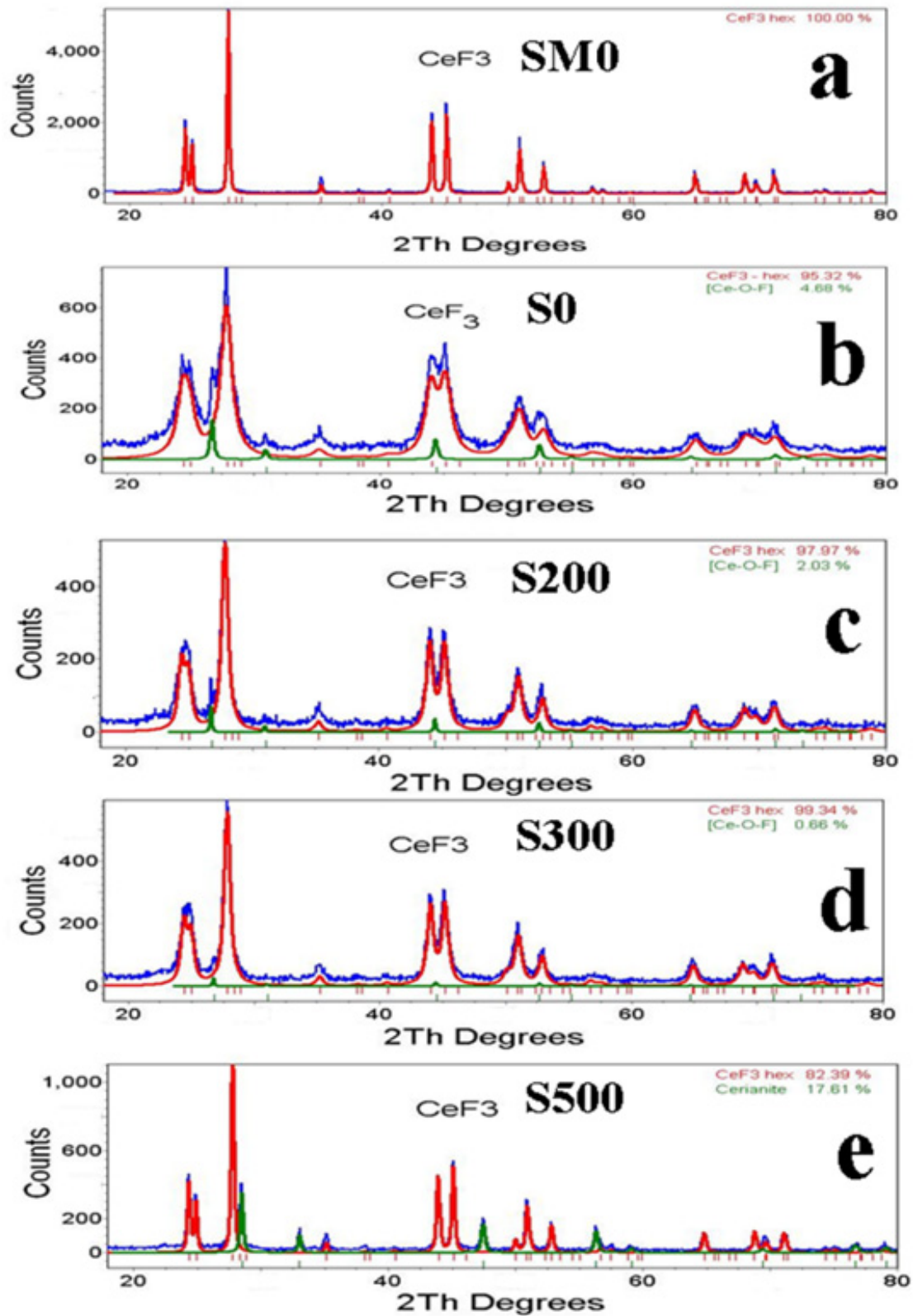
Figure 2. XRD pattern of unannealed (micro and nano powders) (**a**,**b**) and CeF_3 powders air annealed at 200, 300 and 500 °C (**c**–**e**).

Commercial micron powder (Figure 1a) contained one hexagonal phase CeF_3, S.G.: P63/mcm (193), coherent scattering region (CSR) = 87 (3) nm, periods a = 7.129 (4) Å, c = 7.285 (5) Å, ρ = 6.125 (4) g/cm³. (PDF No. 01-089-1933, periods a = 7.13 Å, c = 7.29 Å, ρ = 6.119 g/cm³). The unannealed NP contained two phases: hexagonal phase CeF_3, S.G.: P63/mcm (193); content $\approx$ 95 wt%, CSR $\approx$ 8 nm, periods a = 7.12(2) Å, c = 7.29(2) Å, ρ = 6.15(4) g/cm³, quantitative texture refinement parameters: R_b = 2.339, R_{exp} = 9.92, R_{wp} = 12.67 (PDF No. 01-089-1933, periods a = 7.13 Å, c = 7.29 Å, ρ = 6.119 g/cm³) and impurity cubic phase [Ce-O-F] or [Ce-F], content $\approx$ 5%(weight), SCR = 31 (3) nm, period a = 5.76 (2) Å, ρ = 6.07 (5) g/cm³, R_b = 3.260, R_{exp} = 12.90, R_{wp} = 16.49. The results were processed using a compound similar in composition to CeOF (PDF No. 01-075-0249, S.G.: Fm-3m, cubic, period a = 5.703 Å, ρ = 6.271 g/cm³). The phase composition and lattice parameters of samples S200 and S300 annealed at 200 and 300 °C remained practically unchanged and the CSR size increased from 8 to 12 nm. [Ce-O-F] or [Ce-F], traces 1–2% (wt.). Crystal lattice parameters and CSR size of samples S200 and S300 are given in Table 1.

Table 1. Crystal lattice parameters and CSR dimensions of the hexagonal-phase CeF_3 in annealed samples of S200 and S300.

Sample	$CeF_{3\ hex}$			
	Concentration, % *	CSR, nm	Period, Å	ρ, g/cm³
S200	$\approx$98	15(2)	a = 7.121(3) c = 7.278(3)	6144(2)
S300	>99	16(2)	a = 7.124(3) c = 7.282(3)	6136(2)

* phase [Ce-O-F] or [Ce-F], about 1–2 wt.% (PDF card No. 01-075-0249, S.G.: Fm-3m, cubic, period a = 5703 Å, ρ = 6271 g/cm³).

Annealing of sample S0 at 500 °C (Table 2) resulted in the formation of cerium oxide cubic strata NPles (Cerianite CeO_2, S.G.: Fm-3m (225), map PDF No. 00-034-0394, period a = 5.4113 Å, ρ = 7.215 g/cm³), comparable in size CSR with hexagonal CeF_3 NPles (CeF_3, S.G.: P63/mcm (193) map PDF No. 01-089-1933, periods a = 7.13 Å, c = 7.29 Å, ρ = 6.119 g/cm³).

Table 2. Crystal lattice parameters and CSR dimensions of the hexagonal phase of the CeF_3 and cubic phase CeO_2 in the sample S500.

CeF_3				CeO_2			
Concentr., %	CSR, nm	Period, Å	ρ, g/cm³	Concentr.,%	CSR, nm	Period, Å	ρ, g/cm³
$\approx$82	50(2)	a = 7.129(3) c = 7.285(3)	6124(3)	$\approx$18	44(2)	a = 5.411(2)	7.215(3)

In the article in [21], CeF_3 nanoparticles with an average nanocrystal size of 9.6 nm comparable to the NPles (CSR $\approx$ 8 nm) in sample S0, were annealed in air at 350 °C for 1 h and at 500 °C for 6 h. The particle sizes after annealing were 17.6 and 63.7 nm. The CeF_3 NPle sizes in our samples of S300 and S500 annealed in air for 0.5 h were 16 and 50 nm, respectively, indicating approximately the same growth rate of the CeF_3 nanocrystals at a comparable size of the starting particles, regardless of the method of preparation and the degree of agglomeration of the particles. In [21], the authors also recorded the formation of CeO_2 oxide (concentration 30%, particle size 75 nm) during annealing of the sample at a temperature of 500 °C, which is consistent with our XRD data.

The morphological analysis of CeF3 NPles produced in vacuum by PEBE was carried out by us earlier in [12] using low-resolution TEM and high-resolution transmission electron microscopy (HRTEM). Briefly, the produced NPles (Figure 3) were mesoporous agglomerates of particles (agglomerate size: several hundred nm), consisting of amorphous-crystalline particles, from ultrasmall size (2–3 nm) to large particles, 15–16 nm in size, with

an irregular, ellipsoid shape, without a clear cut. The SAED patterns are consistent with a hexagonal-phase structure of CeF_3.
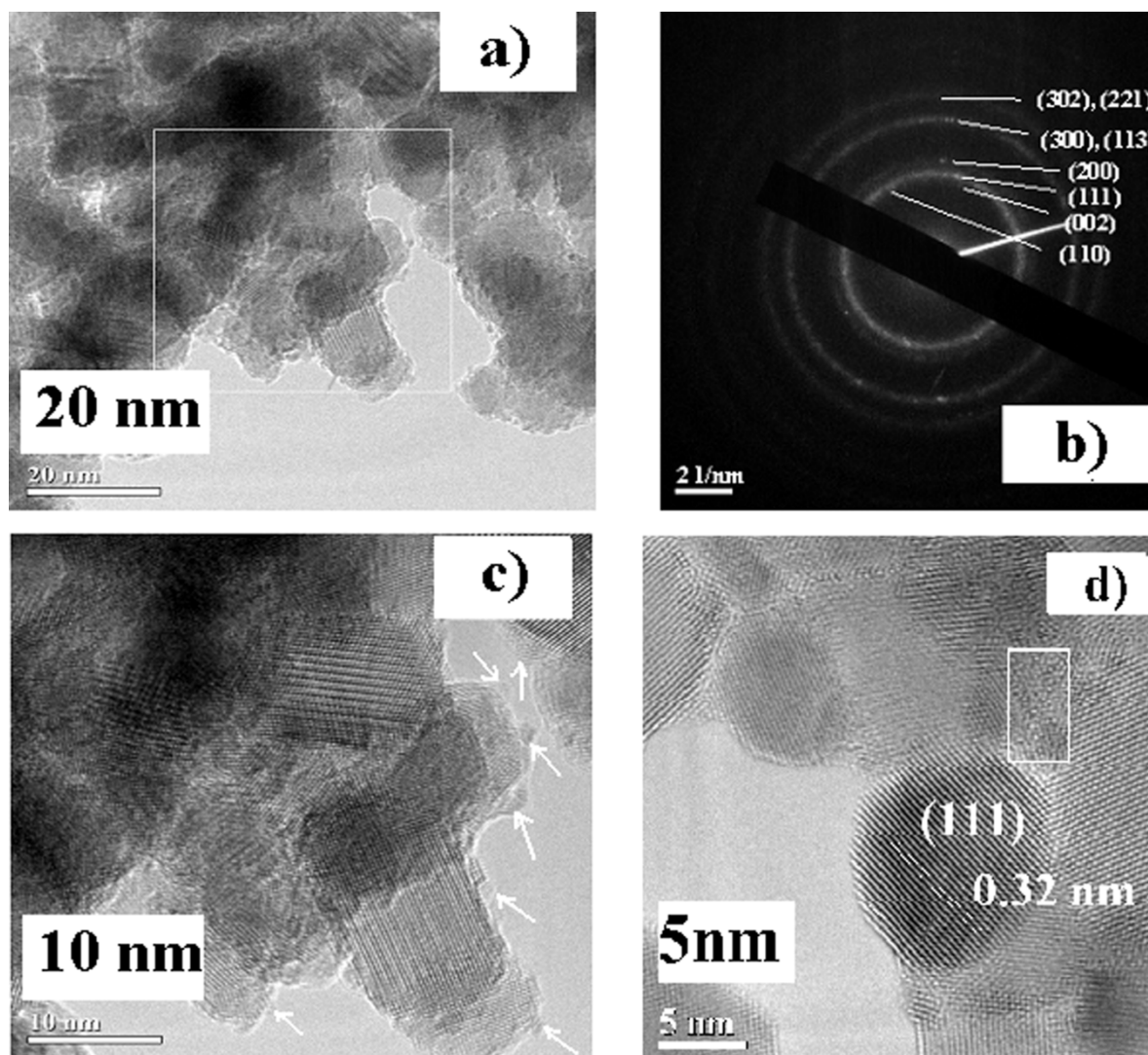
Figure 3. (**a**) TEM; (**c**,**d**) HRTEM images and (**b**) SAED (selected-area electron diffraction pattern) pattern of CeF_3 nanoparticles. The area highlighted by a white rectangle in (**a**) is shown in (**c**). The amorphous area of the sample in (**d**) is marked with a white rectangle [12].

Figure 4 shows isotherms of adsorption–desorption of trifluoride (micro and nano sizes) and their pore-size distribution. The micron commercial powder (target) had a specific surface area (SSA) of 7.2 m^2/g. The nitrogen isotherms of samples S0 and SM0 in Figure 4a,c belong to the IV type with an H3 hysteresis. The SSA and texture parameters of the initial and annealed powders are given in Table 3. The SSA of the non-annealed CeF3 NP (sample S0) is nearly 8-times more than the SSA of the commercial sample SM0. With a smaller pore size, the sample has a significantly larger pore volume. The unimodal pore-size distribution in micron powder (Figure 4d) with a maximum of about 20 nm was transformed in NP into an almost uniformly increasing pore distribution (Figure 2b) in a range of 7.5 to 17 nm. Improved textural parameters of CeF_3 nanopowder indicate its possible use as a nanocontainer for drug delivery, as confirmed by recent studies [12].
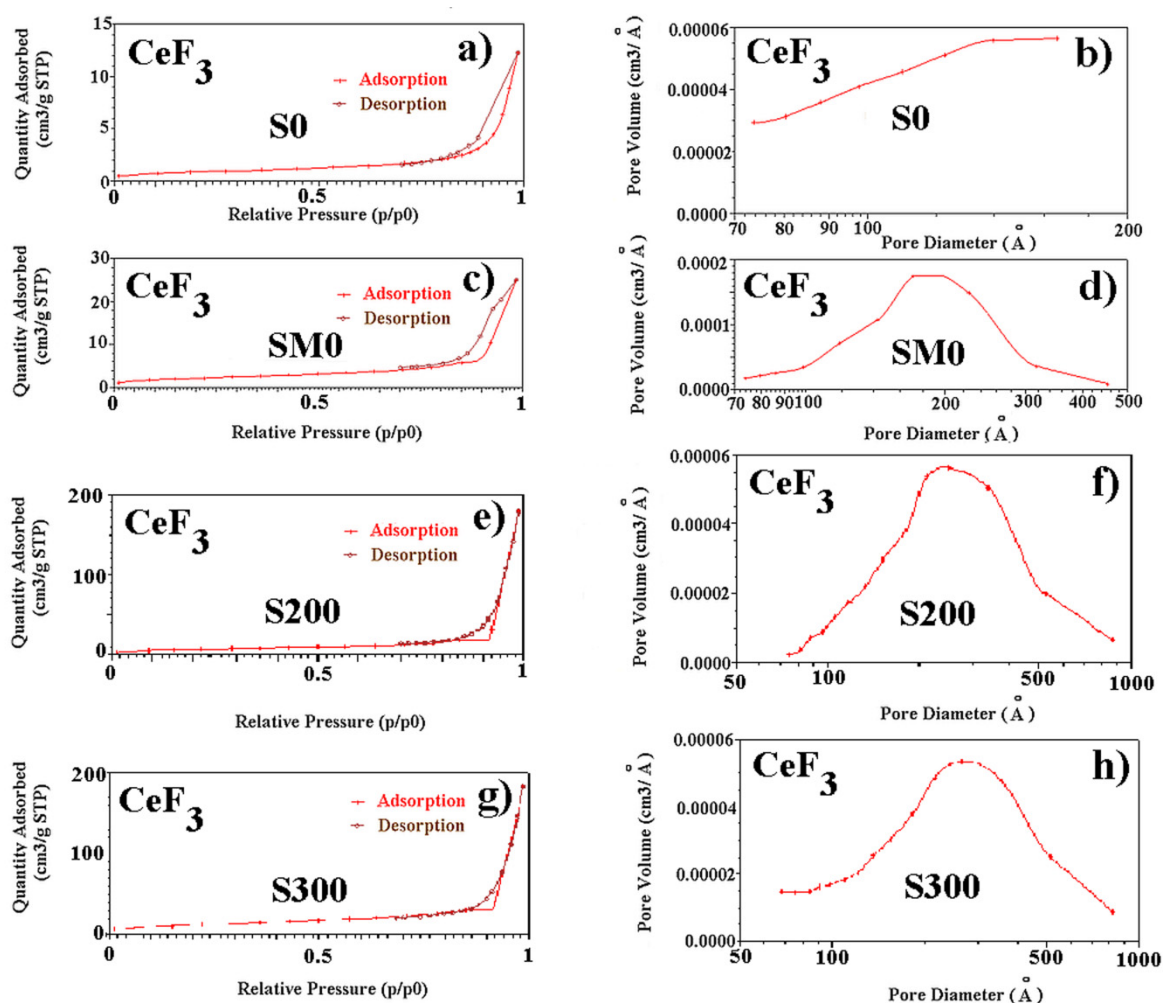
Figure 4. Nitrogen adsorption/desorption isotherms (**a**,**e**,**g**) and pore-size distribution curves (**b**,**f**,**h**) of samples S0, S200, S300 and commercial micron powder Ce F_3 (**c**,**d**), respectively.

Table 3. Texture parameters of non-annealed and air-annealed samples of CeF_3 micro and nano powders.

Samples	SSA (m^2/g)	Pore Size (nm)	Pore Volume (cm^3/g)
SM0	7.2	21.5	0.04
S0	62.0	12.3	0.11
S200	25.1	33.7	0.28
S300	44.5	32.3	0.28

The thermal stability of non-annealed NP and commercial CeF_3 powder was determined using the synchronous DSC-TG method and mass spectral analysis. Figure 5a,b show the DSC-TG synchronous heating curve and H_2O, CO_2 mass spectra of the sample CeF_3 NP and commercial powder in a temperature range 40–1400 °C in argon atmosphere, respectively. Three thermal peaks are visible on the DSC heating curve of CeF3 NP (Figure 5a): endothermic peak *1* (40–250 °C) was caused by evaporation of adsorbed water. Up to a temperature of 730 °C, no thermal changes were observed. The thermal stability of the CeF_3 sample after heating to a temperature 730 °C was disturbed, as indicated by exothermic peak *2* (730–1170 °C). It is probable that exothermic peak *2* could be caused by evaporation the sample impurity—cerium tricarbonate. Exothermic peak *3* (1170 to 1400 °C) (Figure 5a) is associated with the phase transformation of the metastable hexagonal-phase CeF_3 into a more stable x-CeF_3 phase.
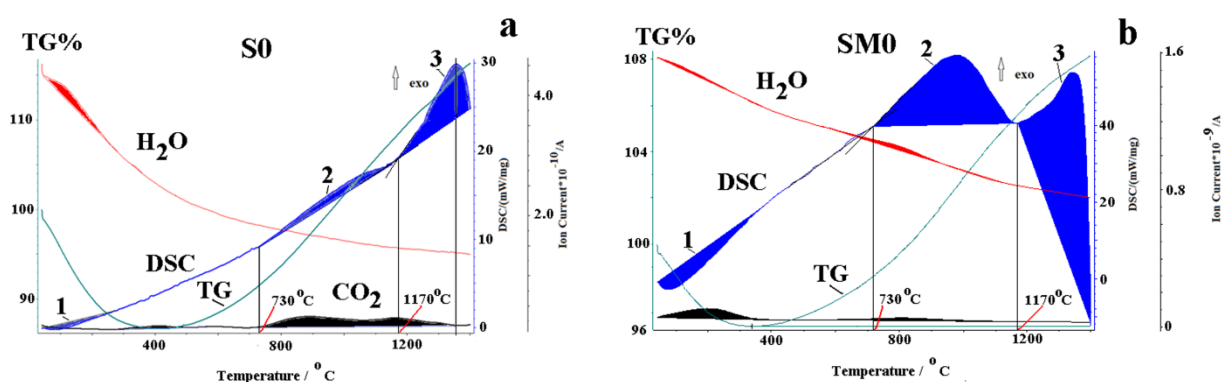
Figure 5. (**a**) Synchronous heating curves (40–1400 °C, Ar) DSC-TG and H_2O, CO_2 mass spectra of CeF_3 NP; (**b**) synchronous heating curves (40–1400 °C, Ar) DSC-TG and H_2O, CO_2 mass spectra of commercial powder CeF_3.

Three corresponding thermal peaks were present on the commercial powder heating thermogram (Figure 5b), which was recorded under the same conditions. The difference between the thermograms of commercial powder and NP was as follows: (a) The decrease in NP mass was associated with the evaporation of H_2O from the porous structure of NP (13%) and continued up to a temperature of 400 °C, while a decrease in the mass of commercial powder (mainly due to CO_2 evaporation), when heated to a temperature of about 350 °C, did not exceed 3.5%, which is consistent with the texture data of both powders in Table 3. A small amount of crystallization water evaporated from the commercial powder at a temperature above ~650 °C. (b) Loss of thermal stability in the nanopowder occurred at a temperature above 725 °C and was accompanied by a large loss of CO_2 (see corresponding CO_2 mass spectrum), while commercial powder lost thermal stability at the lower temperature of 660 °C, with significantly less CO_2 desorption, compared to NP. This difference in the behavior of powders in thermal heating is due to the difference in their production methods—PEBE and the chemical method (technology from Sigma-Aldrich, # 229555). The same appearance temperature of exothermic peak *3* for both powders (~1170 °C) indicates the same, nonvariant type of phase transformation of both powders, probably associated with the formation of an unknown high-temperature CeF_3 phase, as we indicated in [12].

Figure 6 shows the magnetization curves of NP and commercial power CeF_3 annealed in air at a temperature 200, 300 and 500 °C. Curves of magnetization of CeF_3 NP and commercial powder CeF_3 are linear functions in the field. The susceptibility size corresponds to tabular value at a room temperature of 1.1×10^{-6} cm^3/g, i.e., transition to a nanostate did not affect the magnetic behavior of CeF_3. A significant increase in the RTFM response was observed in composite CeO_2/CeF_3 NPles [10]. We did not observe the emergence of a ferromagnetic response at room temperature that can be connected with a lack of the necessary amount of structural defects on borders of grains—"fluoride-oxide", when forming oxide particles of CeO_2 on CeF_3 NPle surface when annealing. However, the formation of an oxide coating on the surface of fluoride particles in CeF3 NP is indicated by a decrease in magnetization of the S500 sample by Figure 6 compared to the magnetization of the remaining samples. Obviously, the occurrence of FM at RT requires high-energy exposure to various types of ionizing radiation (gamma, electrons, X-rays, etc.) on the "fluoride-oxide" interface.

Cathodoluminescence was not excited in the original NP (sample S0), annealed NP (samples S200, S300 and S500) and also in commercial powder (sample SM0). It is curious that PCL was excited in a single crystal sample of CeF_3 [22] during excitation at the CLAVI installation, which we used to excite the cathodoluminescence of powder samples. This circumstance calls for further comment.
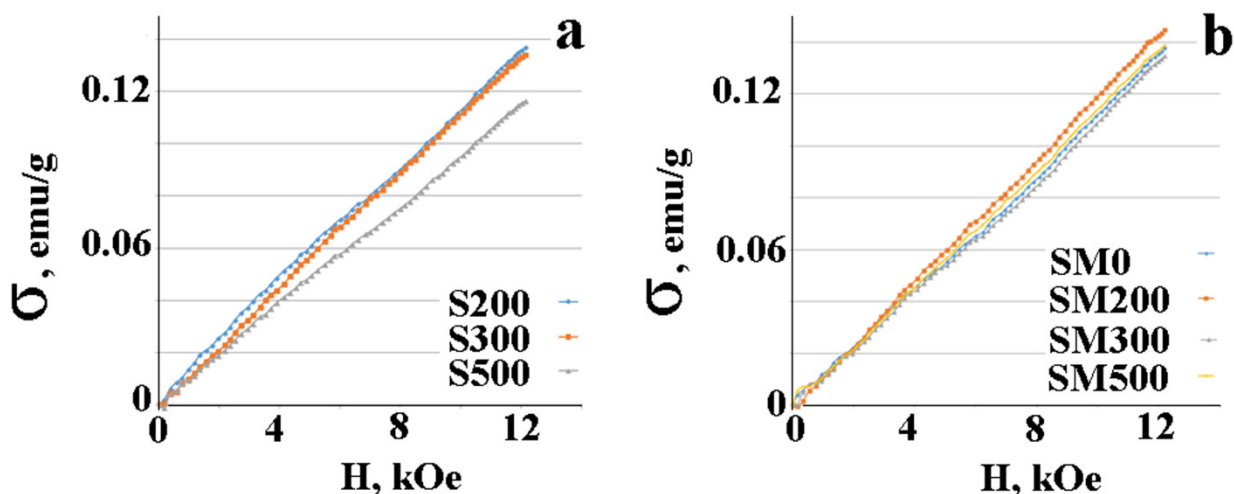
Figure 6. (**a**) Specific magnetization of CeF$_3$ NPles annealed in air at temperatures of 200, 300 and 500 °C; (**b**) specific magnetization of commercial CeF$_3$ powder annealed in air at temperatures of 200, 300 and 500 °C.

Photoluminescence spectra (PL) and deconvolution by the Gaussians of unannealed and annealed samples of CeF$_3$ nanopowder and commercial CeF$_3$ powder at 200, 300 and 500 °C are shown in Figure 7.
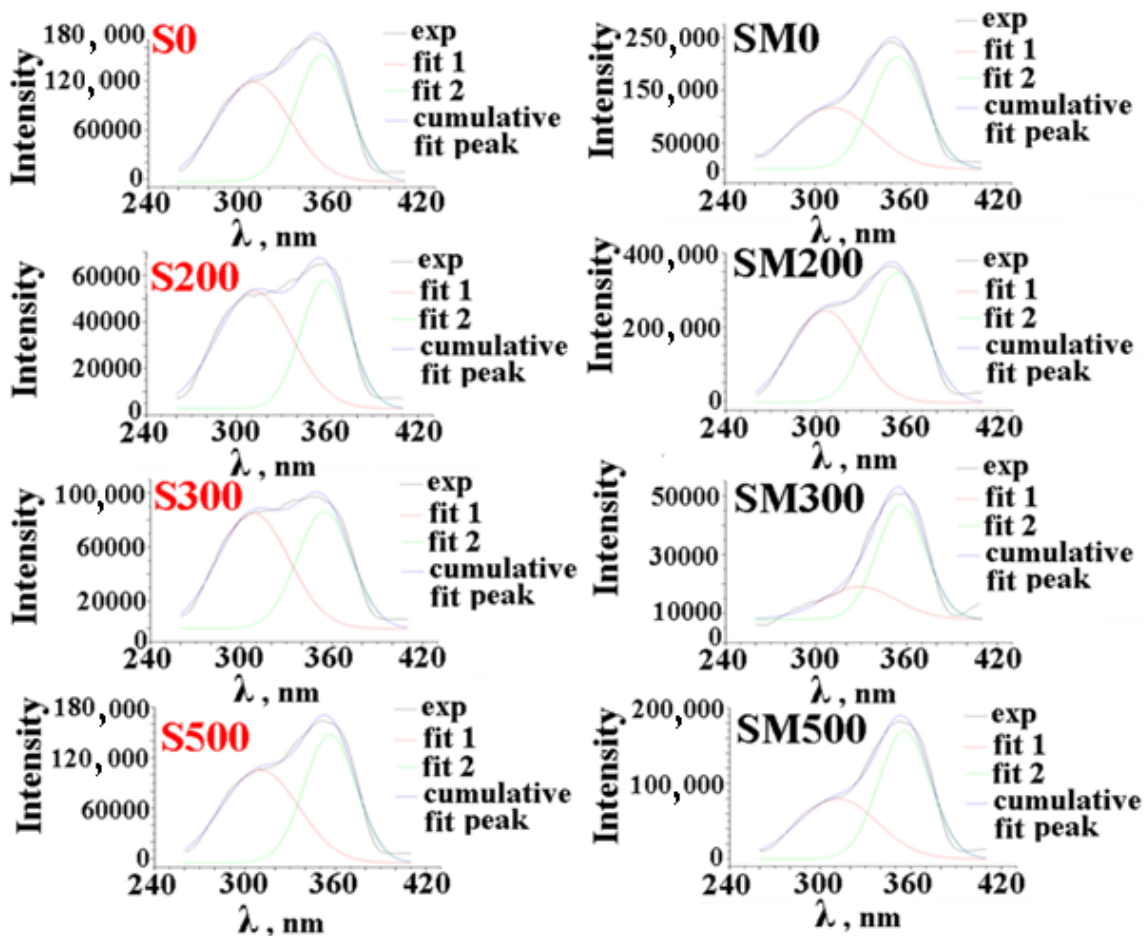
Figure 7. PL spectra NP and commercial powder CeF$_3$ before and after annealing in air at 200, 300 and 500 °C.

The deconvolution parameters are given in Table 4.

Table 4. Deconvolution parameters of PL spectra of CeF$_3$ micro- and nanopowder samples before and after annealing in air in a temperature range of 200–500 °C.

Sample	X1 nm	X2 nm	A1/A2	Sample	X1 nm	X2 nm	A1/A2
S0	309.7	355.1	1.1	SM0	311.1	354.5	0.84
S200	311.4	358.5	1.43	SM200	306.0	353.1	0.86
S300	307.9	354.9	1.29	SM300	328.2	356.2	0.43
S500	310.0	356.3	1.08	SM500	311.5	355.7	0.73

Designations: X1 and X2—position of individual band maxima; A1/A2—area ratio of individual bands.

The micro- and nanopowder spectra contained one wide peak in a range 260 to 390 nm, consisting of two peaks with maxima at ~(308–312) nm (excluding sample SM300) and ~(353–358 nm). The PL spectra of micro- and nanoforms showed opposite trends with respect to the peak intensities of the above A1/A2 peaks. The intensity ratio of all S0–S500 samples was greater than one and vice versa; SM-SM500 micron samples were always less than one. Note also that there is no significant displacement of peaks after annealing both types of powders, regardless of the annealing temperature. Literature data relate both peaks to Ce^{3+} ion emission (transition 5d–4f) [23,24].

The cytotoxicity of non-annealed CeF3 NP with respect to cell cultures was assessed using the following criteria: if the cell viability was reduced by less than 40%, the cytotoxicity was assessed as low; if it was decreased by 40–70%, it was assessed as moderate and if it was decreased by more than 70%—as high. According to the results of the experiment, it was found that when CeF$_3$ and CeF$_3$ nanopowders (from glass) were added to the HeLa tumor culture, the cell viability decreased by 20–35% at all test concentrations (Figure 8).
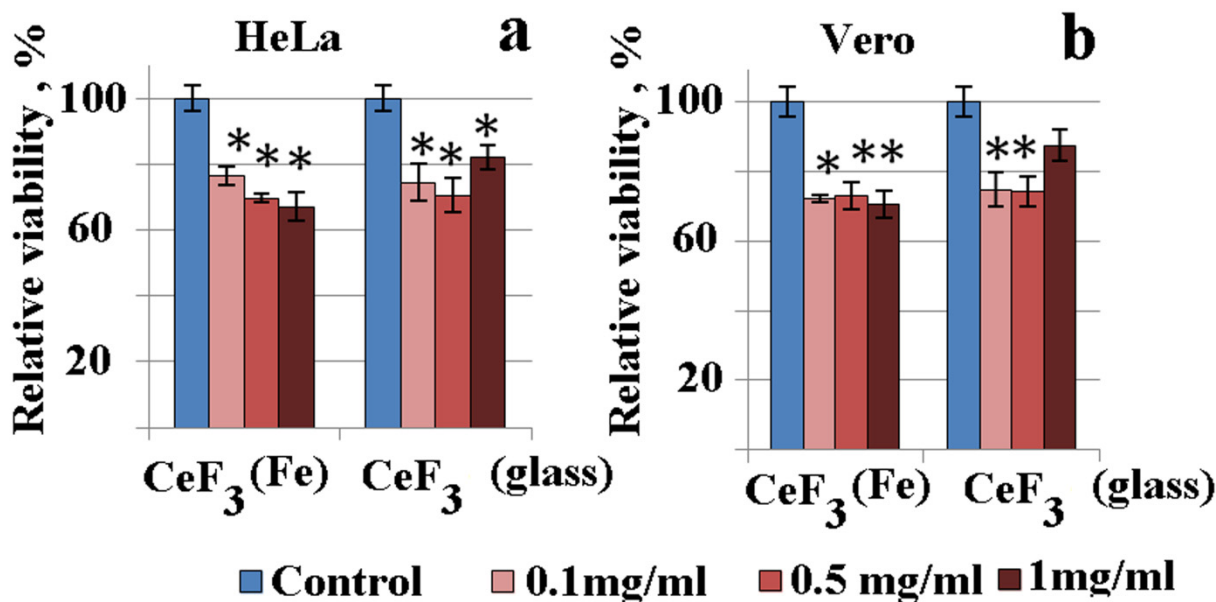
Figure 8. Change in cell viability when adding CeF$_3$ and CeF$_3$ nanopowders (from glass): (**a**) HeLa cell culture; (**b**) Vero cell culture (*-difference with control is significant ($p < 0.05$)).

Cytotoxicity study of CeF3 NP showed that after adding CeF3 NP to non-neoplastic culture Vero (the study used CeF3 NP collected from glass and metal substrates located in the evaporation chamber of the Nanobeam-2 installation [12]), there was a decrease in cell viability at 25–30% at all concentrations, but using CeF3 NP collected from glass substrates only at NP concentrations of equal to 0.1 and 0.5 mg/mL. The lack of cytotoxicity

effect at a higher NP concentration of 1 mg/mL may have been caused by agglomeration of the nanoparticles in suspension, resulting in a decrease in the active surface area of the nanoparticles available to the cells, thus, resulting in a decrease in toxicity of the nanoparticle agglomerates (see Figure 8b).

A cytotoxicity study of CeF_3 nanopowder collected from glass and metal substrates showed low cytotoxicity of fluoride NPles in both tumor and non-tumor cells.

3. Conclusions

Annealing of CeF3 NP in the air led to the formation of two-phase CeF3 NP-CeO_2 at a temperature of 500 °C. The formation of the fluoride–oxide interface was reflected in the magnetic response of the S500 sample. However, the RTFM response did not appear. The volume and pore size of NP after annealing at a temperature of 200–300 °C increased almost 3-times, which makes such powders promising for drug delivery. The textural parameters of the commercial CeF_3 powder (SSA, volume and pore size) are inferior to the corresponding parameters of the nanopowder. All CeF_3 NPs without exception showed low cytotoxicity in relation to tumor and healthy cells. The thermal resistance of the NP was 65 °C higher than that of the micron powder. The NP samples showed a higher PL peak intensity at 308–312 nm compared to the high-energy PL peak intensity in micron powder. No cathodoluminescence was found in both types of samples, regardless of annealing temperature. Mesoporous CeF3 NP, obtained from a micron powder, has prospects for loading, storage, transportation and efficient release of drugs contained in it, i.e., its use as a nanostructured container [25]. The pore size, morphology (SSA) and surface composition of nanoparticles can be controlled by varying the technological parameters in the PEBE method [12].

4. Experimental Section

4.1. Materials

Cerium(III) fluoride micron powder (CeF_3, anhydrous, powder, 99.99% trace metals basis, Sigma-Aldrich, #229555) was used for producing CeF_3 NPles.

4.2. Characterization

The X-ray diffractogram was taken on the D8 DISCOVER diffractometer. Nitrogen adsorption and desorption isotherms were obtained using Micromeritics TriStar 3000 V6.03 A. Thermal analysis was carried out on synchronous thermoanalytic complex NETZSCH STA-409. Magnetic measurements were carried out using a Faraday balance. Photoluminescence spectra (PL) were recorded on an MDR-204 spectrometer with a deuterium lamp DDS-30, with a light filter (0.6–1 μm) and smoothing out the noisy spectra. The cytotoxicity of CeF_3 nanopowders (NP collected from the surface from stainless steel) and CeF_3 (NP collected from glass substrates) was tested in human and animal cell cultures: Vero green monkey cell culture and HeLa human tumor culture. Incubation of cells and preparation of solutions were carried out under sterile conditions in the laminar box BAVnp-01-"Laminar-S"-1,2 LORICA. The cells were cultured in a Sanyo SO_2 incubator (Panasonic) MCO-18AC at 37 C in a 5% SO_2, 95% humidity atmosphere using Igla DMEM culture media (Biolot, Russia) supplemented with 10% fetal calf serum (Biolot, Russia) streptomycin at a dose of 50 μg/mL until monolayer formation. To investigate the effect of NP on viability, cell cultures were placed in 96-well plates of 100 μL each. Culture was carried out for 24 h, then 10 μL NP suspensions were added to the wells at final concentrations of 0.1, 0.5 and 1 mg/mL. No NP was added to the control wells. On day 3, the metabolic activity of the cells was evaluated using an MTT test. Then, 20 μL of MTT dye (tetrazolium dye 3-(4,5-dimethylthiazol-2-yl) -2,5-diphenyl-tetrazolium bromide) was added to the wells and the plates were incubated for 2 h at 37 °C under 5% CO_2. During this time, the MTT dye under the action of NADH-N-dependent oxidoreductases of living cells was reduced into a purple-colored formazan product, the amount of which is proportional to the number of living cells. The precipitated formazan crystals were dissolved in 100 μL of dimethyl

sulfoxide (DMSO) for 20 min at 37 °C. The optical absorbance of dyed DMSO solutions was measured on a Tecan Infinite M200 PRO plate scanner at a wavelength of 570 nm using the Magellan program. The MTT test results were evaluated by comparing the optical density in the test and control wells.

Author Contributions: Conceptualization, V.I.; Investigation, A.M., T.S., O.S., M.A.U., M.U. and M.Z.; Project administration, S.S. All authors have read and agreed to the published version of the manuscript.

Institutional Review Board Statement: Not applicable.

Informed Consent Statement: Not applicable.

Conflicts of Interest: The authors declare no conflict of interest.

References

1. Ackland, K.; Coey, J.M.D. Room temperature magnetism in CeO_2—A review. *Phys. Rep.* **2018**, *746*, 1–39. [CrossRef]
2. Soni, S.; Kumar, S.; Vats, V.S.; Khakhal, H.R.; Dalela, B.; Dolia, S.N.; Kumar, S.; Alvi, P.A.; Dalela, S. Oxygen vacancies and defects induced room temperature ferromagnetic properties of pure and Fe-doped CeO_2 nanomaterials investigated using X-ray photoelectron spectroscopy. *J. Electron Spectrosc. Relat. Phenom.* **2022**, *254*, 147140. [CrossRef]
3. El-Achari, T.; Goumrhar, F.; Drissi, L.B.; Laamara, R.A. Structural, electronic and magnetic properties of Mn doped CeO_2: An ab-initio study. *Phys. B Condens. Matter* **2021**, *601*, 412443. [CrossRef]
4. Chernyshev, A.P. Oxygen vacancy concentration in nanoobjects of $CeO_{2-\delta}$: Effects of characteristic size, morphology, and temperature. *Mater. Sci. Eng. B* **2021**, *274*, 115481. [CrossRef]
5. Saifi, M.A.; Seal, S.; Godugu, C. Nanoceria, the versatile nanoparticles: Promising biomedical applications. *J. Control. Release* **2021**, *338*, 164–189. [CrossRef]
6. Nyoka, M.; Choonara, Y.E.; Kumar, P.; Kondiah, P.P.D.; Pillay, V. Synthesis of Cerium Oxide Nanoparticles Using Various Methods: Implications for Biomedical Applications. *Nanomaterials* **2020**, *10*, 242. [CrossRef]
7. Ivanov, V.K.; Shcherbakov, A.B.; Baranchikov, A.E.; Kozik, V.V. *Nanocrystalline Cerium Dioxide: Properties, Preparation, Application*; Tomsk University Press: Tomsk, Russia, 2013.
8. Shcherbakov, A.B.; Zholobak, N.M.; Ivanov, V.K. Biological, biomedical and pharmaceutical applications of cerium oxide. In *Cerium Oxide (CeO_2): Synthesis, Properties and Applications*; Metal Oxides Series; Elsevier: Amsterdam, The Netherlands, 2020. [CrossRef]
9. Shcherbakov, A.B.; Zholobak, N.M.; Baranchikov, A.E.; Ryabova, A.V.; Ivanov, V.K. Cerium fluoride nanoparticles protect cells against oxidative stress. *Mater. Sci. Eng. C* **2015**, *50*, 151–159. [CrossRef] [PubMed]
10. Morozov, O.A.; Pavlov, V.V.; Rakhmatullin, R.M.; Semashko, V.V.; Korableva, S.L. Enhanced Room-Temperature Ferromagnetism in Composite CeO_2/CeF_3 Nanoparticles. *Phys. Status Solidi RRL* **2018**, *12*, 1800318. [CrossRef]
11. Ilves, V.G.; Sokovnin, S.Y. Production and Studies of Properties of Nanopowderson the Basis of CeO_2. *Nanotechnol. Russ.* **2012**, *7*, 213–226. [CrossRef]
12. Ilves, V.G.; Sokovnin, S.Y.; Uimin, M.A. Properties of cerium (III) fluoride nanopowder obtained by pulsed electron beam evaporation. *J. Fluor. Chem.* **2022**, *253*, 109921. [CrossRef]
13. Lu, J.; Xue, Q.; Ouyang, J. Thermal properties and tribological chracterictics of CeF_3 compact. *Wear* **1997**, *211*, 15–21. Available online: https://www.halide-crylink.com/wp-content/uploads/2020/06/12-Thermal-properties-and-tribological-characteristics-of-CeF-3-compact.pdf (accessed on 24 November 2022). [CrossRef]
14. Wang, J.; Ansari, A.A.; Malik, A.; Syed, R.; Ola, M.S.; Kumar, A.; AlGhamdi, K.M.; Khan, S. Highly Water-Soluble Luminescent Silica-Coated Cerium Fluoride Nanoparticles Synthesis, Characterizations, and In Vitro Evaluation of Possible Cytotoxicity. *ACS Omega* **2020**, *5*, 19174. [CrossRef] [PubMed]
15. Chaput, F.; Lerouge, F.; Bulin, A.L.; Amans, D.; Odziomek, M.; Faure, A.C.; Monteil, M.; Dozov, I.; Parola, S.; Bouquet, F.; et al. Liquid-Crystalline Suspensions of Photosensitive Paramagnetic CeF_3 Nanodiscs. *Langmuir* **2019**, *35*, 16256. [CrossRef]
16. Dong, H.; Du, S.R.; Zheng, X.Y.; Lyu, G.M.; Sun, L.D.; Li, L.D.; Zhang, P.Z.; Zhang, C.; Yan, C.H. Lanthanide Nanoparticles: From Design toward Bioimaging and Therapy. *Chem. Rev.* **2015**, *115*, 10725. [CrossRef]
17. Bartha, C.; Secu, C.; Matei, E.; Negrila, C.; Leca, A.; Secu, M. Towards a Correlation between Structural, Magnetic and Luminescence Properties of CeF_3:Tb^{3+} Nanocrystals. *Materials* **2020**, *13*, 2980. [CrossRef]
18. Shen, X.; Li, T.; Chen, Z.; Geng, Y.; Xie, X.; Li, S.; Yang, H.; Wu, C.; Liu, Y. Luminescent/magnetic PLGA-based hybrid nanocomposites: A smart nanocarrier system for targeted codelivery and dual-modality imaging in cancer theranostics. *Int. J. Nanomed.* **2017**, *12*, 4299–4322. [CrossRef]
19. Sokovnin, S.Y.; Balezin, M.E. Production of Nanopowders Using Nanosecond Electron Beam. *Ferroelectrics* **2012**, *436*, 108–111. [CrossRef]

20. Ilves, V.G.; Sokovnin, S.Y.; Zuev, M.G.; Uimin, M.A.; Rähn, M.; Kozlova, J.; Sammelselg, V. Effect of annealing on structural, textural, thermal, magnetic, and luminescence properties of calcium fluoride nanoparticles. *Phys. Solid State* **2019**, *61*, 2200–2217. [CrossRef]

21. Mishra, S.; Jeanneau, E.; Bulin, A.L.; Ledoux, G.; Jouguet, B.; Amans, D.; Belsky, A.; Daniele, S.; Dujardin, C. A molecular precursor approach to monodisperse scintillating CeF_3 nanocrystals. *Dalton Trans.* **2013**, *42*, 12633. [CrossRef]

22. Snigireva, O.A.; Solomonov, V.I. Role of the Ce^{2+} ions in cerium fluoride luminescence. *Phys. Solid State* **2005**, *47*, 1443–1445. [CrossRef]

23. Zhu, L.; Li, Q.; Liu, X.; Li, J.; Zhang, Y.; Meng, J.; Cao, X. Morphological Control and Luminescent Properties of CeF_3 Nanocrystals. *J. Phys. Chem. C* **2007**, *111*, 5898. [CrossRef]

24. Chylii, M.; Loghina, L.; Kaderavkova, A.; Slang, S.; Rodriguez-Pereira, J.; Frumarova, B.; Vlcek, M. Morphology and optical properties of CeF_3 and CeF_3:Tb nanocrystals: The dominant role of the reaction thermal mode. *Mater. Chem. Phys.* **2021**, *260*, 124161. [CrossRef]

25. Vivero-Escoto, J.L.; Slowing, I.I.; Trewyn, B.G.; Lin, V.S.-Y. Mesoporous silica nanoparticles for intracellular controlled drug delivery. *Small* **2010**, *6*, 1952–1967. [CrossRef] [PubMed]